A Second Look At The $\Delta\theta$ Systematic Effect And The Moon Shadow

by **Morgan O. Wascko**

August 10, 2000

Abstract

Monte Carlo simulations are used to estimate the angular resolution and systematic pointing error due to late light of Milagrito. These are used in a simulation to determine their effect on the location and width of the moon shadow. This is compared to data. The overall angular resolution of Milagrito (no nFit cut) is found to be 1.4°.

1 Introduction

The reconstruction of Milagrito events is affected by late light from the shower front. This late light systematically biases reconstructed showers towards the horizon, increasing as a function of the zenith angle of the incident particle. Figure 1 illustrates the effect. Shower front particles cause Cherenkov emission in a cone of opening angle 41°. Some of the light is emitted downwards and is detected promptly by the nearby PMTs. Some of the light, however, is emitted approximately horizontally, and travels across the pond before being detected by more distant PMTs. Since the Cherenkov light travels at c/n in the pond, which is much slower than the shower particles themselves in the pond, this horizontal light arrives later than Cherenkov emission from the shower front particles themselves as they pass through the far end of the pond. These late PMT hits, if not rejected by the angle fitter, will cause the shower plane fits to be skewed towards the horizon systematically. This will tend to make θ_{Fit} larger than θ, causing the $\Delta\theta$ versus θ systematic pointing error we see in the Milagrito data.

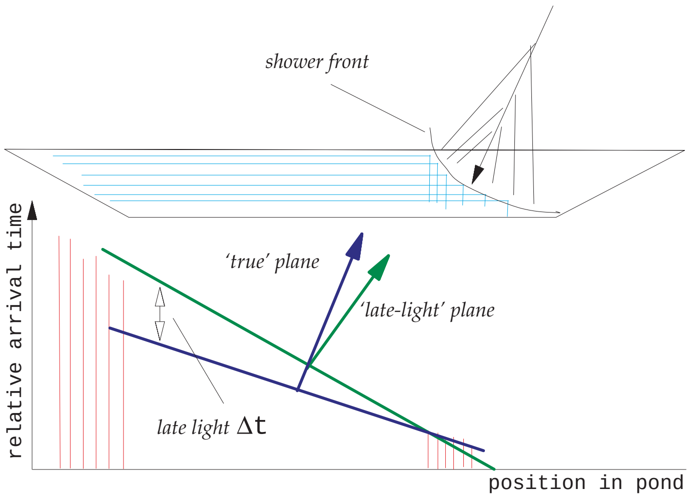

Figure 1: Simplified diagram of the cause of the $\Delta\theta$ versus θ systematic. The shower front particles cause Cherenkov emission vertically and horizontally, as shown in the upper part of the diagram. The lower part shows the relative arrival times of hits in pond PMTs. If only the prompt hits are used, the fitted shower plane would be given by the blue plane. But if the late hits are used in the fit, the fitted shower plane would be more like the green plane.

This memo describes work I've done to study this phenomenon, and its effect on the angular resolution. For the analyses in this work, I use the Milagrito Monte Carlo events thrown by Joe and Stefan. They consist of 873,326 proton showers, 500,000 He helium showers and 50,000 CNO Nitrogen showers. Using these events I find ΔAngle for each pond trigger, where ΔAngle is defined as the space angle difference between the throw angle and the reconstructed angle. Note that ΔAngle can only be defined for Monte Carlo events. This is the truest measure of the angular resolution of detector. I then fit the ΔAngle distributions to Gaussian functions in seven nFit bands. ΔAngle is found to be a strong function of nFit, as expected. I separately use the same Grito Monte Carlo events to estimate the $\Delta\theta$ systematic pointing error due to late light. I use a new definition of $\Delta\theta$, which characterizes the systematic offset well, as described below. The updated versions of both ΔAngle and $\Delta\theta$ are used in a simulation of the moon shadow. The $\Delta\theta$ parameters are used to correct the Milagrito moon shadow data. The simulation is compared to the data to find the actual systematic pointing error and angular resolution.

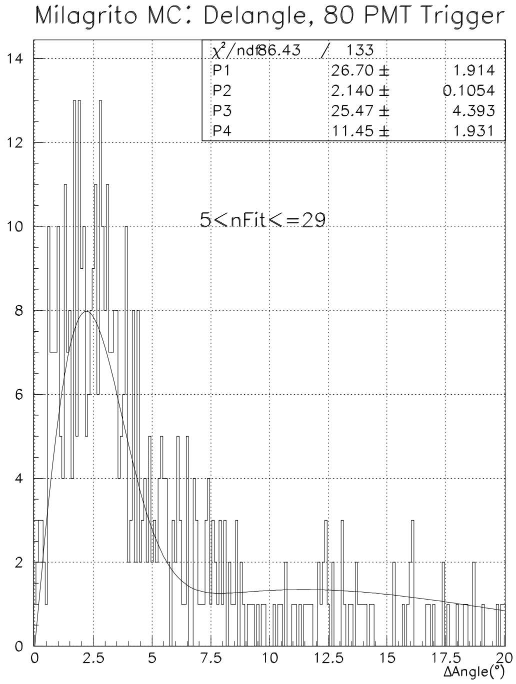

Figure 2: Typical ΔAngle plot. The ΔAngle histogram is fit to the function $P1 \cdot re^{-r^2/2(P2)^2} + P3 \cdot r \cdot e^{-r^2/2(P4)^2}$, with the fit parameters shown. The wider Gaussian accounts for the long tail nicely, while the thinner Gaussian accounts for the peak of the distribution.

2 ΔAngle

Previously, I assumed that ΔAngle is distributed in θ-ϕ space as a two dimensional Gaussian. The projection in r of a two-dimensional, symmetric Gaussian is $r \times Gaussian$, and so we expect the ΔAngle distributions to be well fit by $r \times Gaussian$. This was found to be the case, with the exception of some long tails that were more prevalent in the low nFit bands than in the high. To account for this, I take ΔAngle to be the projection in r of a sum of two dimensional Gaussian distributions, allowing the width and overall normalizations of the Gaussians to vary independently. The use of two Gaussians yields better fits to the data, shown by lower χ^2 of the fits using two Gaussians. Table 1 shows the improvement in χ^2 gained by using two Gaussians rather than one. With two Gaussians in the fits, one accounts for the peaks and the other for the tails of the distributions. (See Figure 2 for a detailed example of this. The rest of the fits are shown in Figure 9.) With this method, ΔAngle is now characterized by two widths, both of which are found to be a strong function of nFit, as shown by Figure 6. The ΔAngle vs. nFit plots are fit with exponentials, and the parameters of the fits are used in the simulations as the angular resolution of the detector.

3 $\Delta\theta$ vs. θ

The $\Delta\theta$ vs. θ systematic offset is a tendency to reconstruct showers with larger zenith angles than the actual zenith angles of the incident primaries due to late light in the shower fronts. To elucidate this effect, I define a new parameter. I project a unit vector in the direction of the incident particle's momentum onto the x-y axis of the pond. The y-axis of the pond coordinate system lies 24.5° west of north and the x-axis lies 24.5° north of east. I then define two parameters ζ_x and ζ_y, as follows:

$$\zeta_x = \sin^{-1}(\sin\theta \cdot \cos\phi) \tag{1}$$

$$\zeta_y = \sin^{-1}(\sin\theta \cdot \sin\phi) \tag{2}$$

Figure 3 illustrates the definitions of the new parameters. (In the text, I will use ζ with no subscript to mean *both* ζ_x and ζ_y.) For each Monte Carlo event, I calculate $\Delta\zeta = \zeta_{Fit}$ - ζ_{Thrown}, and plot $\Delta\zeta$ as a function of ζ. These are then fit to a straight line (see Figures 10 through 13). This parameterization is superior to the one used in the last memo on this subject because it is not biased at zenith as before. However, because the Monte Carlo events currently are thrown only out to 45°, there is an "edge effect" at large angles. This is because it is possible for primary events below 45° to be reconstructed above 45°, but there are no events from primaries above 45° to get reconstructed below 45°. This will lead to an exaggeration of the systematic offset near the 45°, which gets worse as the magnitude of the offset, or the width of ΔAngle, gets larger. Edge effects notwithstanding, the Monte Carlo predicts that the systematic offset is a function of nFit, as shown in Figure 7.

Figures 10 through 13 show the $\Delta\zeta$ vs. ζ fits. Figures 10 and 11 show $\Delta\zeta$ vs. ζ, or the systematic offset as a function of incident angle. Figures 12 and 13 show $\Delta\zeta$ vs. ζ_{Fit}, or the systematic offset as a function of the reconstructed angle. All fits were generated using the same Monte Carlo events. The $\Delta\zeta$ vs. ζ plots can be thought of as the systematic offset itself, since they show the systematic pointing error as a function of the true incident angle. The $\Delta\zeta$ vs. ζ_{Fit} plots can be used as the correction of the systematic offset, since they give the offset as a function of the fitted angle.

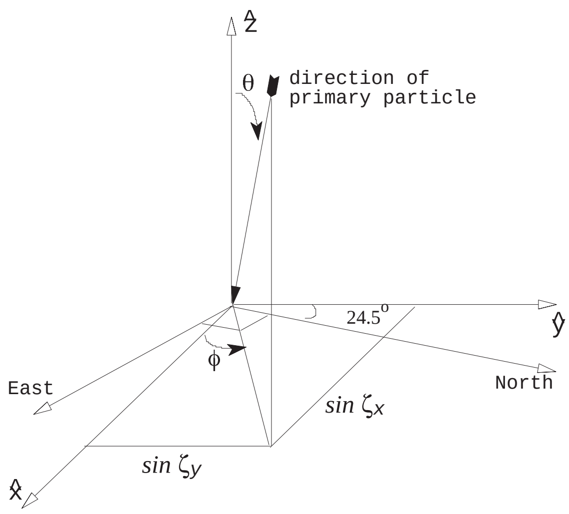

Figure 3: Diagram of the definitions of the parameters ζ_x and ζ_y. Each is the projection of a unit vector in the direction of the primary particle onto the x or y axis.

It is interesting to note that the two parameters, ζ_x and ζ_y, affect the moon shadow differently. This stems from the fact that the majority of the moon data come from the southern part of the sky. This means that most events in the moon shadow data yield negative values for ζ_y, whereas they are symmetric about ζ_x=0. As shown in Figures 10 through 13, the $\Delta\zeta$ systematic offset tends to increase a positive ζ and decrease a negative ζ, so that the effect of the systematic on a set that is distributed about 0, like ζ_x, is to spread the shadow but cause no net offset. In the case of ζ_y, on the other hand, the data are mostly negative, and so the effect is a net offset towards smaller ζ_y along with spreading the shadow. Because of this, the δ offset of the moon shadow can be corrected with just a ζ_y correction, but using both ζ_y and ζ_x corrections should also tighten the moon shadow.

4 Application to the Moon Shadow

The results of the above analyses are used in the simulation of the moon shadow. I generate a moon shadow by throwing events from the moon's direction and then subtracting them from a simulated background. The energy and species of the primary particle are selected randomly from the proper distributions, as is nFit. Starting with the moon's position for a given day and time, I first apply the geomagnetic deflection. This is done as a function of rigidity for the three species of primary particles, assuming a dipole magnetic field whose dipole moment points in the direction of the true magnetic south pole. The resulting deflected direction is taken as the incident direction of the cosmic ray, and this direction is smeared using the ΔAngle distributions and offset using the $\Delta\zeta$ fits. This accounts for the angular resolution of the detector and the systematic offset due to late light.

Over the course of a transit, the offset in declination, δ, due to the magnetic field is much smaller than the angular resolution of the detector. This is due to the direction of the geomagnetic field and the fact that the moon passes nearly symmetrically across the δ component of the field. Thus, the only measurable net offset due to geomagnetic deflection is in right ascension, α, although the filed does smear the moonshadow in δ. It is the $\Delta\theta$ systematic offset that noticeably shifts the shadow of the moon in the δ direction. Thus, applying the reverse offset to the data, event by event, should correct the $\Delta\theta$ systematic offset, and sharpen the shadow.

Figure 4 shows the results of applying the $\Delta\theta$ correction to the data. In terms of reversing the systematic offset of the moon shadow, the current parameterization undercorrects slightly in the high nFit region, and overcorrects slightly in the low nFit region, but the overall effect is quite good as seen in Figure 4. Figure 5 shows the deficit of events as a function of distance from the expected center of the moon shadow. In each plot, the expected deficit is gotten by calculating the event density at the moon's nominal position and multiplying that by the area of the moon. Note that it is slightly different for the corrected and uncorrected data, but that the two are consistent. The $\Delta\theta$ correction does not significantly improve the width of the deficit, however it does yield a more significant deficit.

5 Conclusions

The offset of the position of maximum deficit of the Milagrito moon shadow is due to the combined effects of the geomagnetic deflection and the $\Delta\theta$ vs.θ systematic. The systematic effect caused by late light is absent from the Milagro Moon Shadow, as expected. The α offset is due to the geomagnetic deflection of cosmic rays, but $\Delta\theta$ vs. θ systematic is needed to explain the net δ offset. This offset can be corrected, event by event. If the deficit of events due to the shadow of the moon is fit to a single Gaussian, the result indicates an overall angular resolution of 1.4^{o}.

nFit Band	*One Gaussian*		*Two Gaussians*		
nFit	χ^2	*ndf*	χ^2	*ndf*	%
6-29	169.4	135	86.43	133	51.18
30-35	134.4	94	78.36	92	57.95
36-41	104.7	86	56.74	84	59.10
42-50	91.71	75	57.27	73	59.42
51-63	80.29	66	52.13	64	62.11
64-93	58.43	57	31.73	55	69.99
94+	51.49	38	38.37	36	86.75

Table 1: **Change in χ^2 of the ΔAngle fits for each nFit band.** The last column is the percentage of the total area comprised by the first (smaller σ) Gaussian.

nFit Band	ζ_x		ζ_y	
nFit	ζ_x	$\zeta_x Fit$	ζ_y	$\zeta_y Fit$
6-29	0.03741	0.09800	0.01469	0.09662
30-49	0.02808	0.03373	0.03178	0.04004
50-79	0.01861	0.02137	0.01582	0.02238
80-109	0.01421	0.01411	0.007465	0.09131
110-149	0.01761	0.01886	0.01366	0.01461
150+	0.008416	0.01227	0.01082	0.01383

Table 2: Behavior of $\Delta\zeta_x$ and $\Delta\zeta_y$ for each nFit band. The values of the parameterizations of the $\Delta\zeta$ vs. ζ systematic offset. Shown are the values of the forward and reverse parameterizations. Please feel free to use these numbers in future Milagrito data analyses.

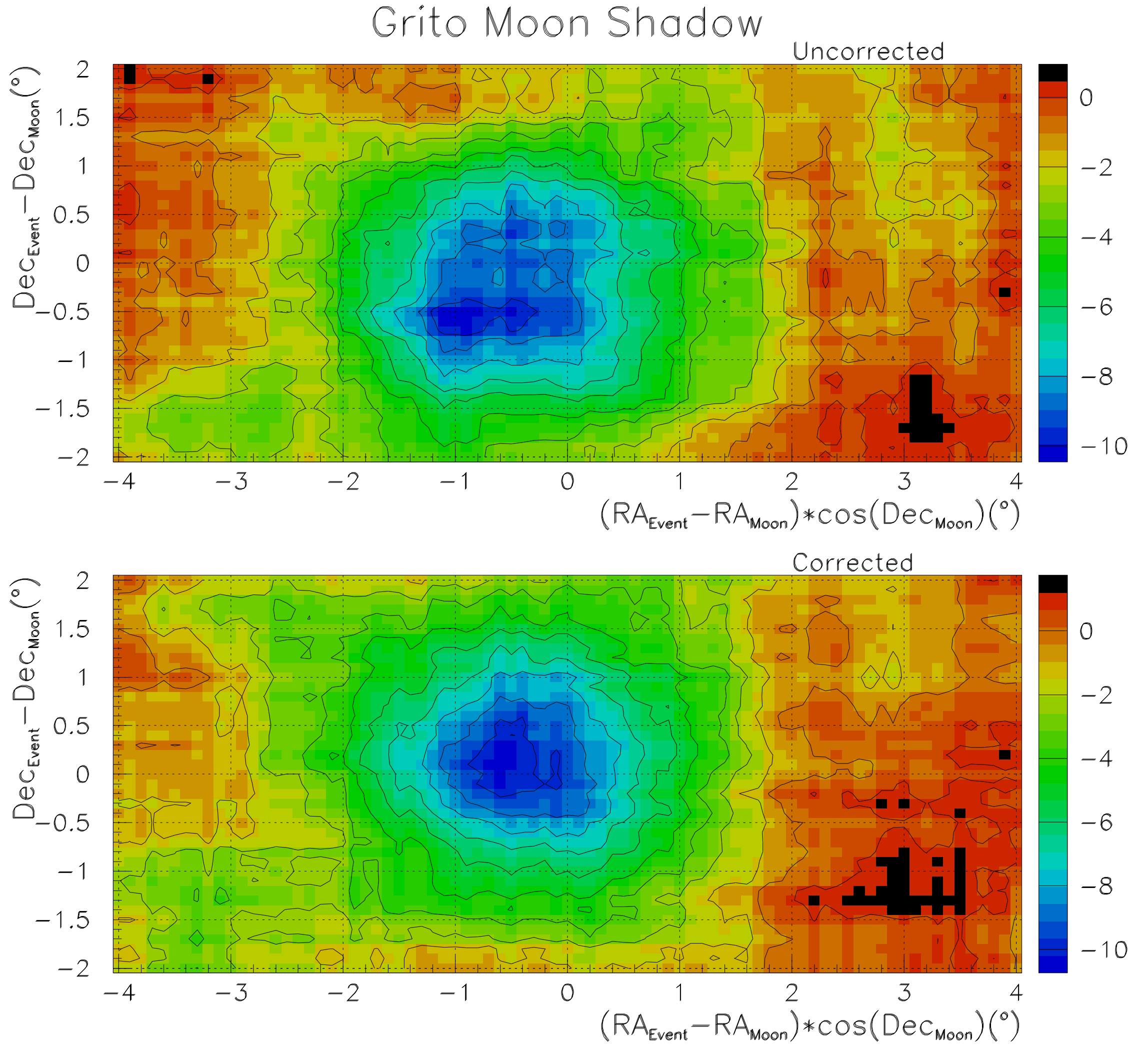

Figure 4: The Milagrito moon shadow. Both plots are comprised of data up to $\theta = 45^o$. The data were corrected for the $\Delta\theta vs.\theta$ offset, event by event, in the bottom plot. The upper plot is uncorrected. Both plots were smoothed using a square bin 2.1^o on a side.

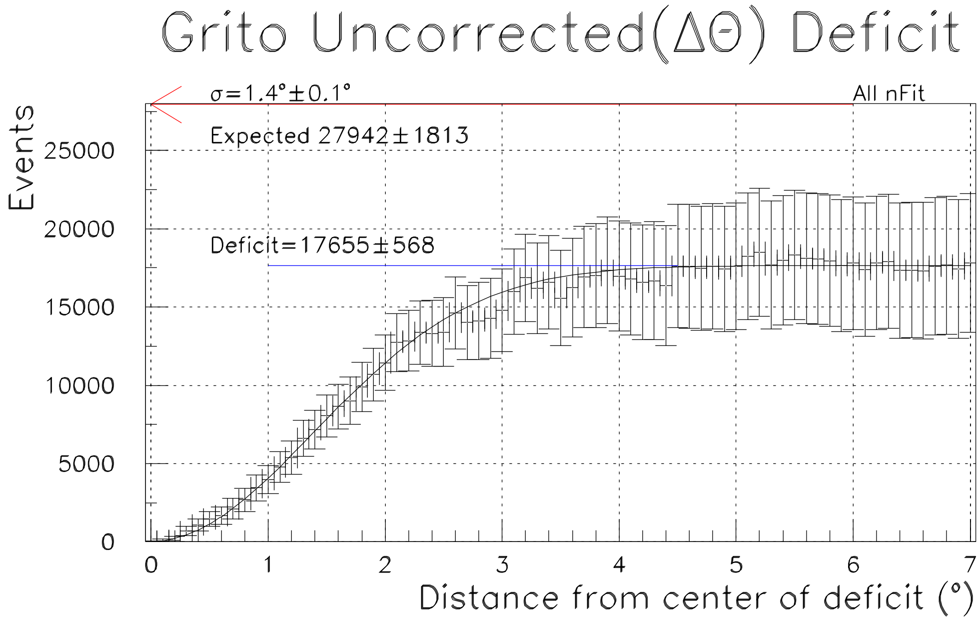

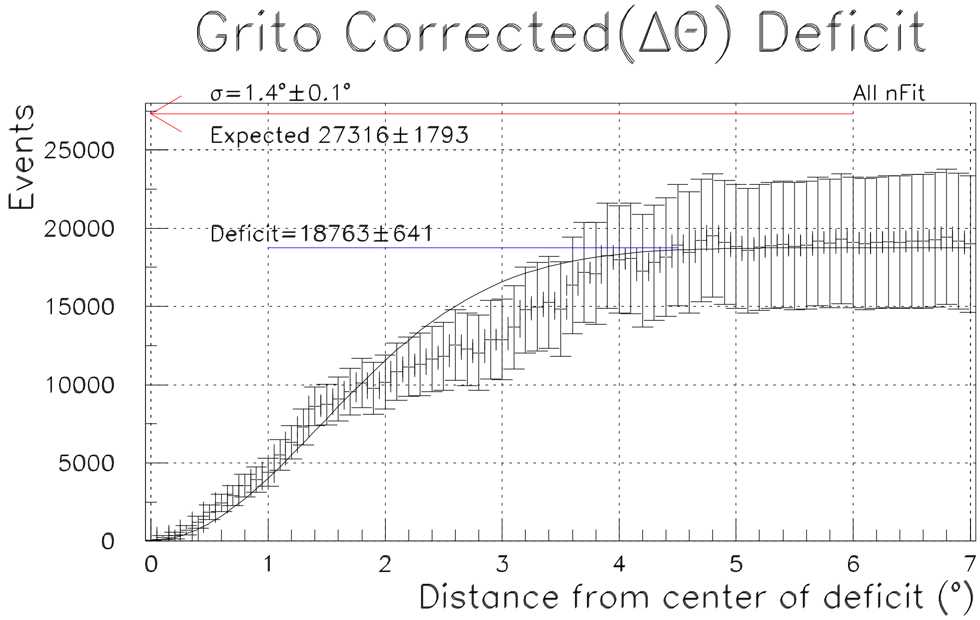

Figure 5: Deficit of events measured as a function of the angular distance from the center of the expected position of the shadow of the moon. The $\Delta\theta vs.\theta$ corrections lead to a more significant deficit, but not to a noticeable improvement in the width of the deficit. Each plot is fit to a constant minus a Gaussian, $P1 - P2 \cdot e^{-\theta^2/2(P3)^2}$. The errors given for the deficit and the width come from this fit.

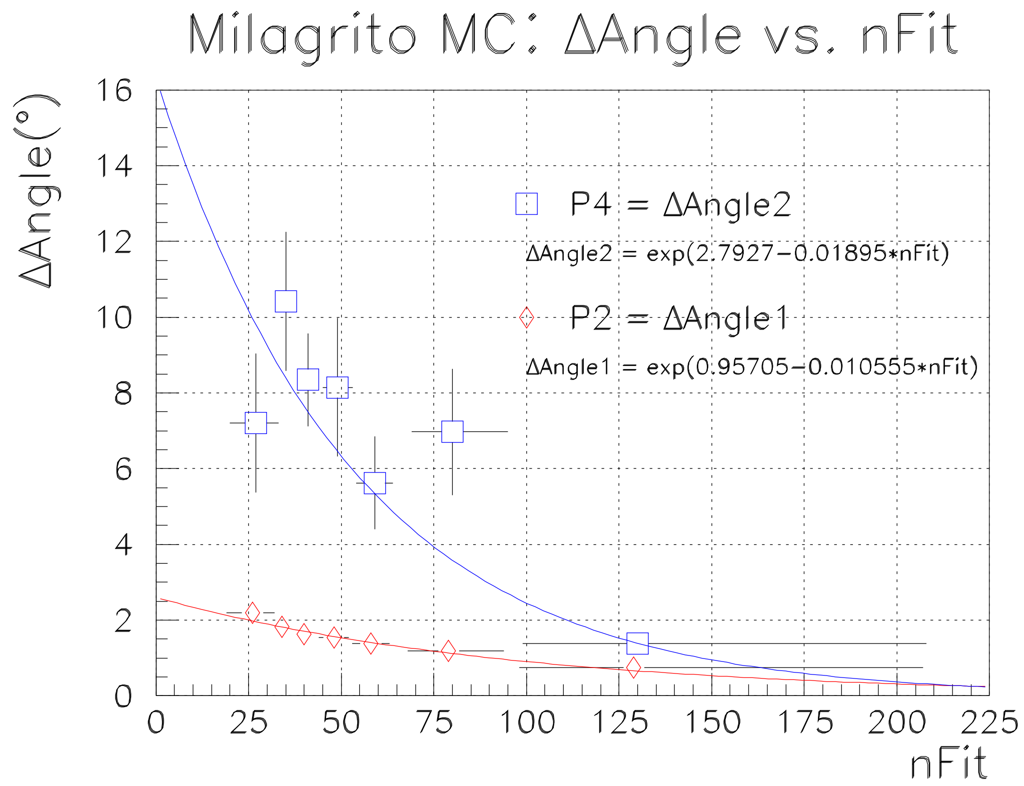

Figure 6: The delangle vs. nFit plot. On the abscissa, the position of the point is placed at the median value of nFit, and the error bars represent the band containing 90% of the data for that nFit band.

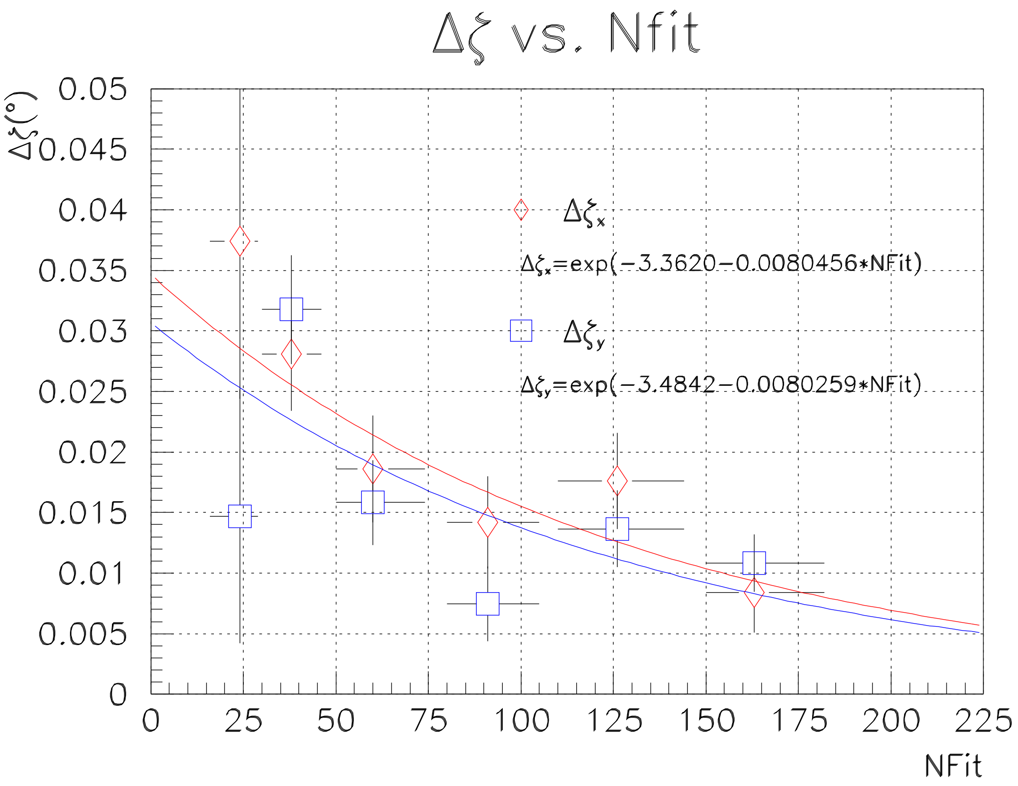

Figure 7: $\Delta\zeta$ values versus nFit. These values are used in the simulation of the moon shadow.

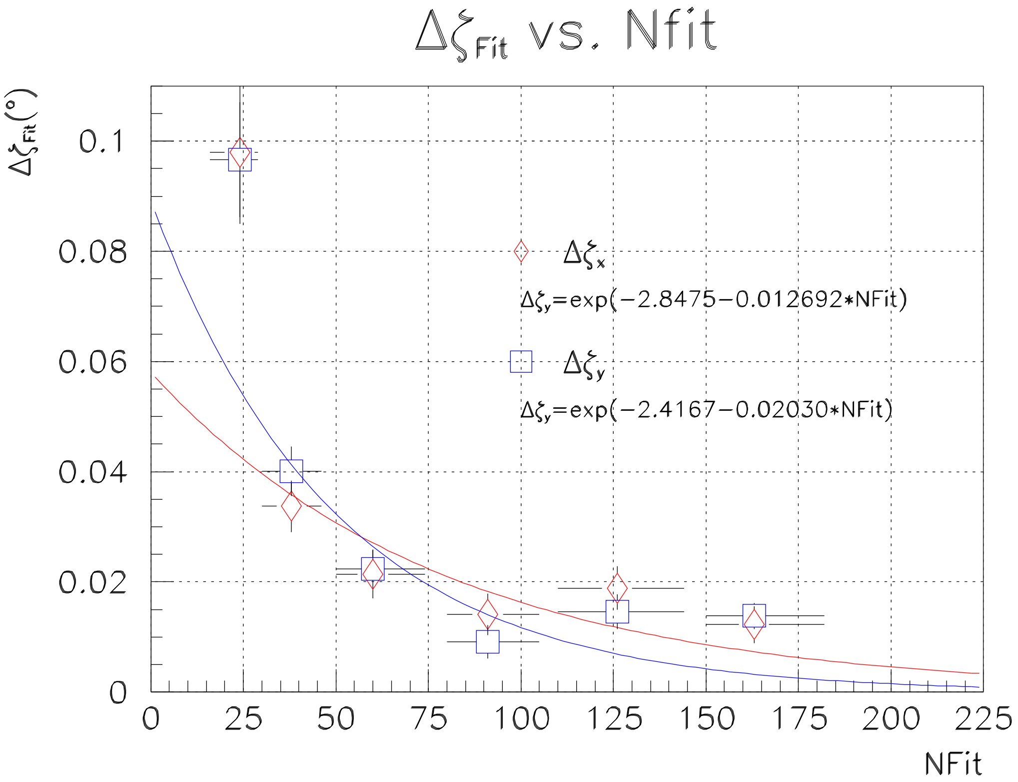

Figure 8: $\Delta\zeta_{Fit}$ values versus nFit. These values are used to correct the $\Delta\theta vs.\theta$ systematic offset in the data, and in the simulation of the shadow of the moon.

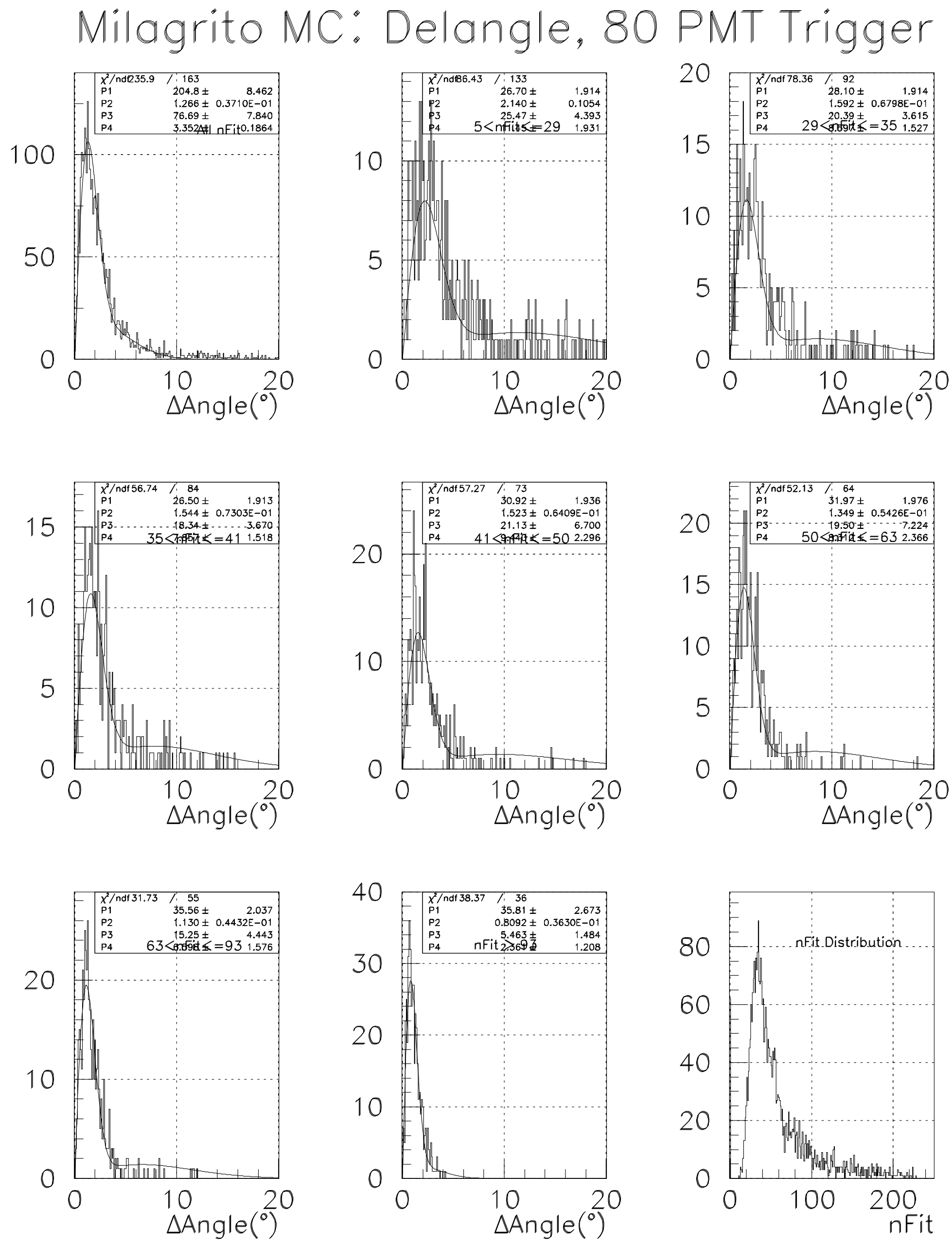

Figure 9: The delangle plots for each nFit band. Shown also is the delangle plot for all events and the nFit distribution.

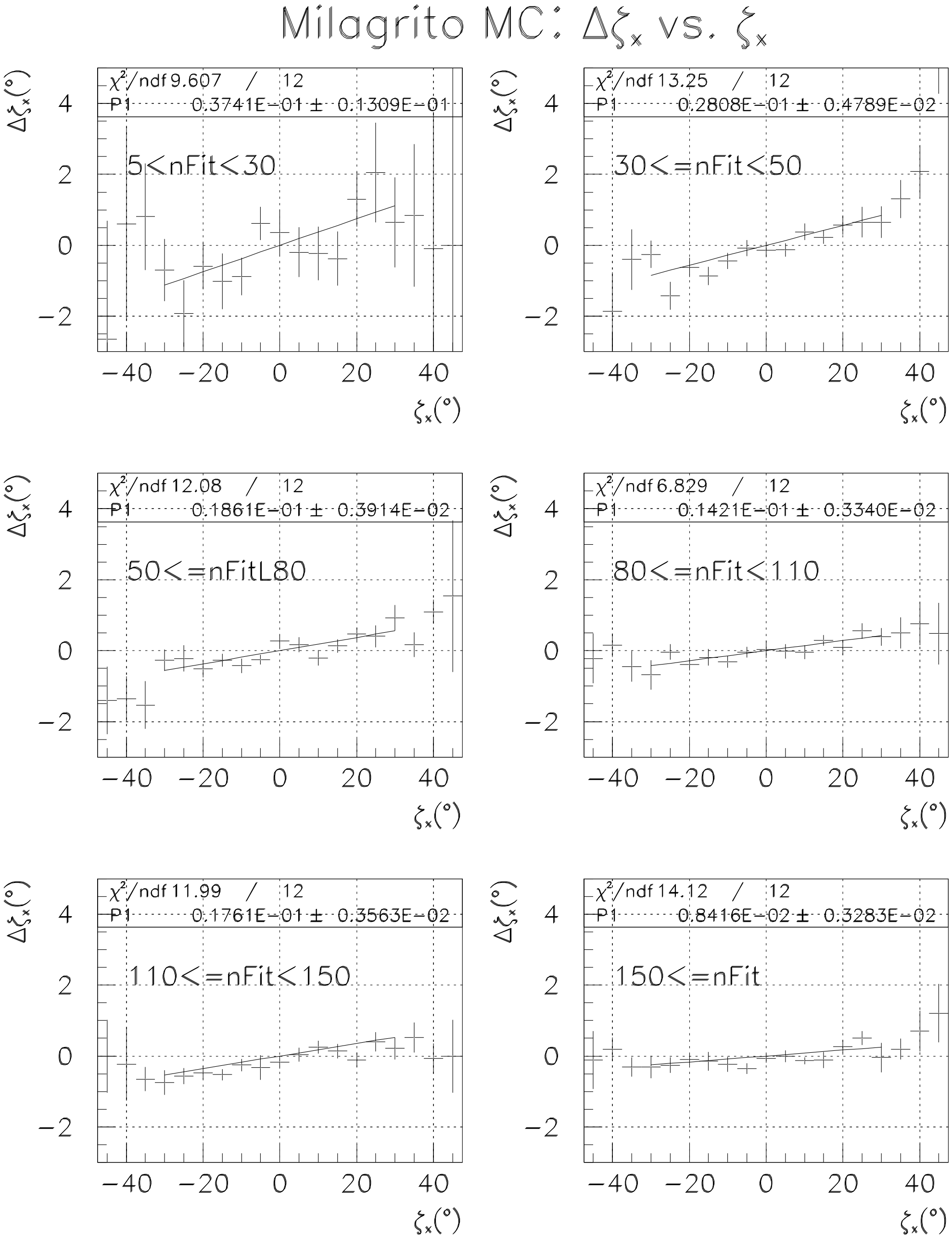

Figure 10: The $\Delta\zeta_x$ *vs.* ζ_x plots for each nFit band. $\Delta\zeta_x = \zeta_{xFit} - \zeta_x$.

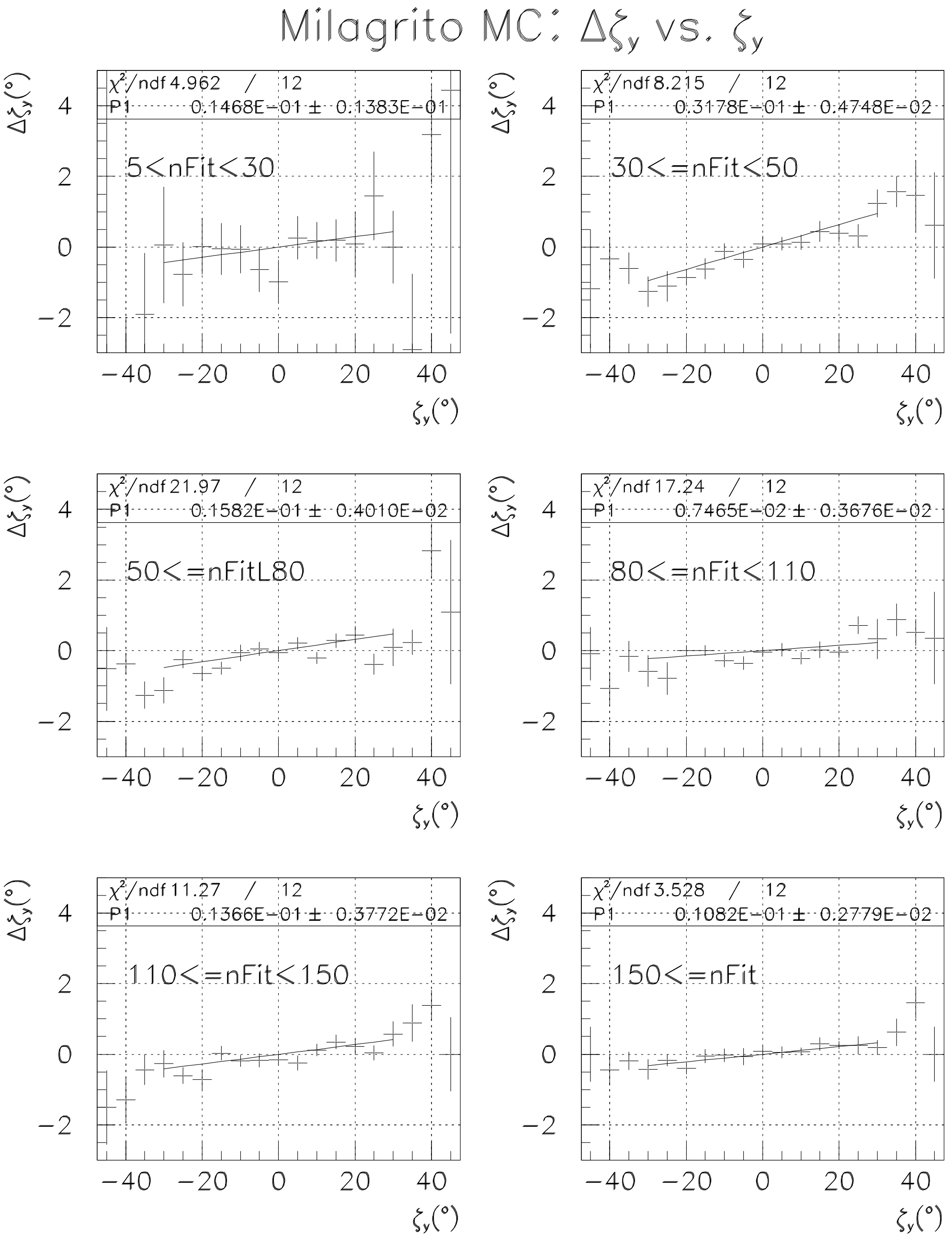

Figure 11: The $\Delta\zeta_y$ $vs.$ ζ_y plots for each nFit band. $\Delta\zeta_y = \zeta_{yFit} - \zeta_y$.

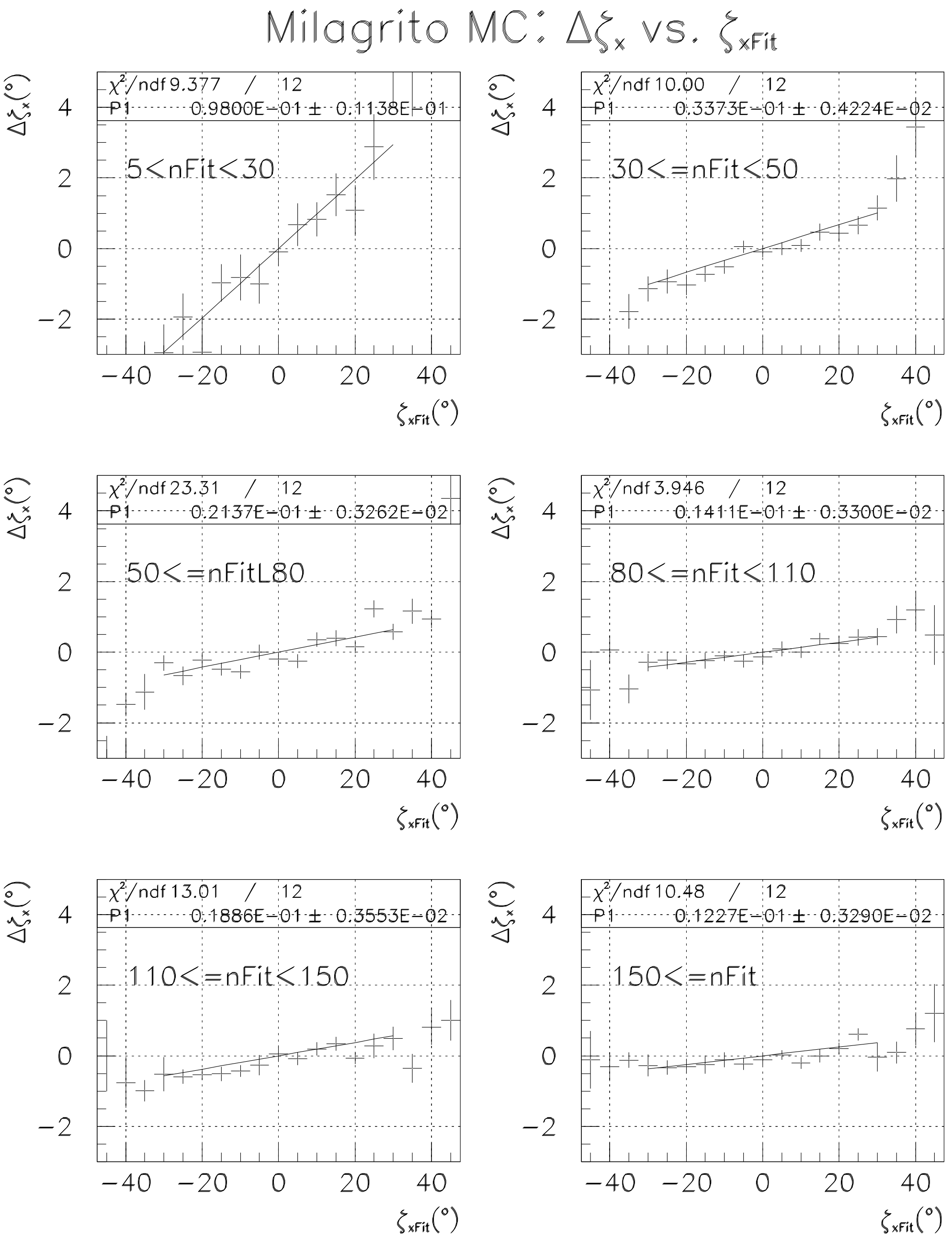

Figure 12: The $\Delta\zeta_x$ *vs.* ζ_{xFit} plots for each nFit band. $\Delta\zeta_x = \zeta_{xFit} - \zeta_x$.

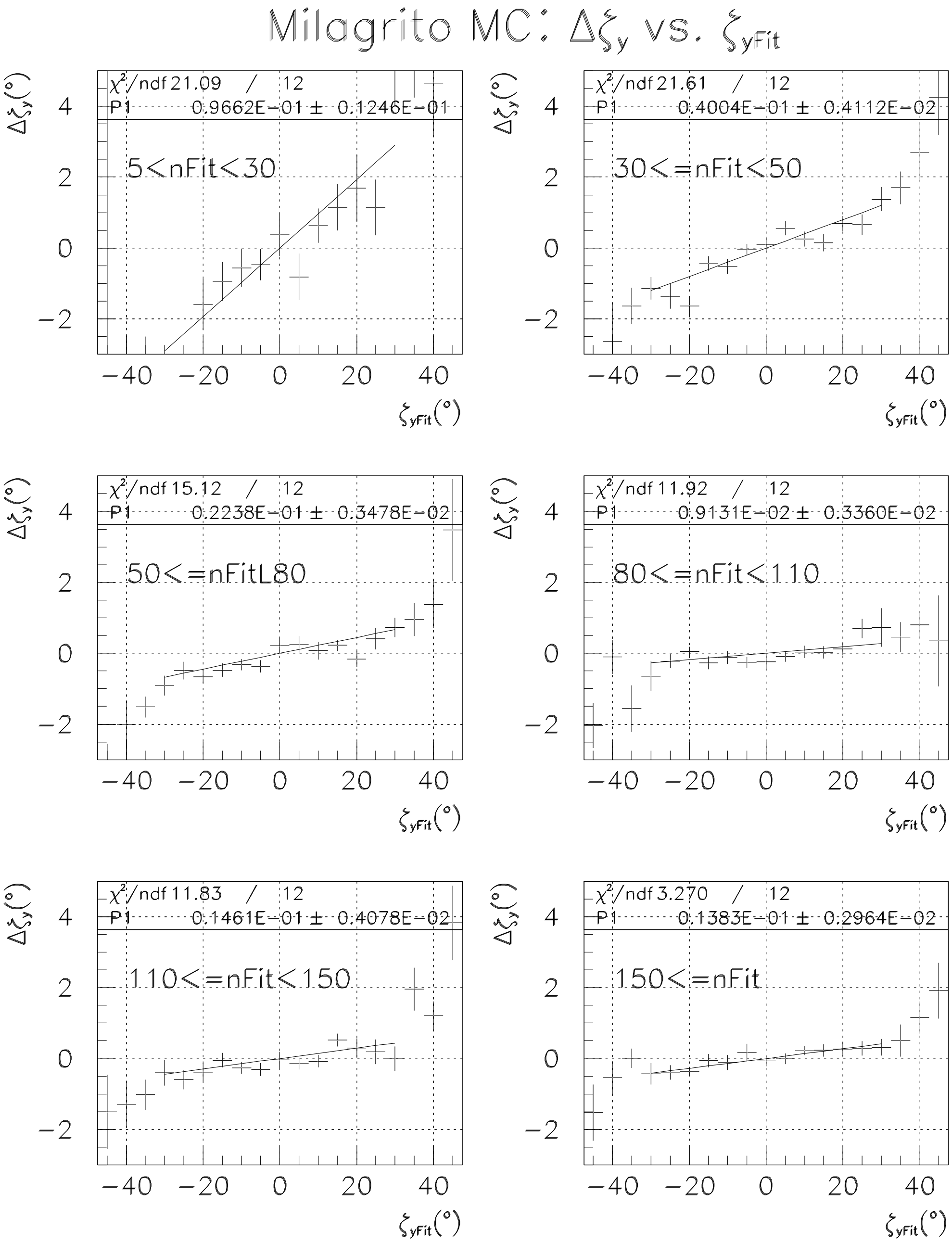

Figure 13: The $\Delta\zeta_y$ *vs.* ζ_{yFit} plots for each nFit band. $\Delta\zeta_y = \zeta_{yFit} - \zeta_y$.